Guiding Electrical Current in Nanotube Circuits Using Structural Defects: A Step Forward in Nanoelectronics

Jose M. Romo-Herrera,[†] Mauricio Terrones,[†] Humberto Terrones,[†] and Vincent Meunier[‡,*]

[†]Advanced Materials Department and National Laboratory for Nanoscience and Nanotechnology Reseearch (LINAN), IPICYT, Camino a la Presa San José 2055, Col. Lomas 4ª Sección, San Luis Potosí 78216, México, and [‡]Oak Ridge National Laboratory, P.O. Box 2008, Oak Ridge, Tennessee 37831-6367

ABSTRACT Electrical current could be efficiently guided in 2D nanotube networks by introducing specific topological defects within the periodic framework. Using semiempirical transport calculations coupled with Landauer—Buttiker formalism of quantum transport in multiterminal nanoscale systems, we provide a detailed analysis of the processes governing the atomic-scale design of nanotube circuits. We found that when defects are introduced as patches in specific sites, they act as bouncing centers that reinject electrons along specific paths, *via* a wave reflection process. This type of defects can be incorporated while preserving the 3-fold connectivity of each carbon atom embedded within the graphitic lattice. Our findings open up a new way to explore bottom-up design, at the nanometer scale, of complex nanotube circuits which could be extended to 3D nanosystems and applied in the fabrication of nanoelectronic devices.

KEYWORDS: carbon nanotube · nanolectronics · defect · electronic properties · quantum transport

Current trends in manufacturing indicate that electronic device miniaturization at the nanoscale faces important challenges using conventional top-down approaches. For example, the assembly of nanocircuits from nanoscale components such as nanowires (1D) and nanoclusters (0D) to form useful circuit nanoelements is plagued by a number of important roadblocks and difficulties. In that respect, the hierarchical assembly of molecular building blocks into ordered arrays has been a recent subject of intense development. These assemblies could involve DNA and RNA (biological blocks),[1−3] nanoparticles (0D blocks),[4−6] and inorganic nanowires (1D blocks).[7−9] Carbon nanotubes (CNTs) are particularly appealing candidates for a bottom-up approach to design novel electronic devices. This is due in part to their conducting or semiconducting behavior and ballistic transport properties (as they possess coherence length larger than their typical physical length). Notably, fundamental electronic components based on isolated nanotubes have already been reported.[10−14] A further step was achieved with 1D blocks (inorganic nanowires), where a single crossbar can act as nanoscale avalanche photodiodes[15] or programmable nonvolatile memory devices.[16] A 3 × 1 nanowire (Si or GaN) network (3 nodes) has been reported to perform as AND or NOR logic gates,[17] and a 4 × 4 network (16 nodes) was constructed to work as an addressable decoder nanosystem.[18] Specifically, Zhong *et al.*[18] modified well-defined cross points of the network at the molecular level to define address codes that enable nanowires input lines to be turned on and off.

Recently, different architectures of ordered networks built using defect-free 1D blocks (e.g., nanotubes) have been described in the literature,[19,20] including a general mathematical algorithm to design different types of architectures to theoretically characterize them.[19] A CNT-based nonvolatile random access memory (RAM) has been proposed for noncovalent networks configurations.[21] Experimentally, *noncovalent* 2D networks (with 3 to 12 nodes) were obtained using CNTs.[22] Recent and efficient methods to assemble inorganic nanowires into stacked (non covalent) ordered arrays using the Langmuir−Blodgett technique,[8] complemented by the coalescence (neighboring CNTs that merge at their contact point) property of CNTs[23−25] suggest the possibility of experimentally generating *covalently bonded* 2D and 3D CNTs networks.

While defect-free systems are often considered the most desirable, the introduction of defects in the CNTs sp^2 lattice is known to potentially lead to unusual properties and novel nanodevices.[26] Defects have been studied in isolated nanotubes such as vacancies,[27] generalized Stone-Wales (SW),[26,28] add-dimers,[29] and 5−7 pair defects.[30,31] Some of these defects can

*Address correspondence to meunierv@ornl.gov.

Received for review September 24, 2008 and accepted November 06, 2008.

Published online November 20, 2008.
10.1021/nn800612d CCC: $40.75

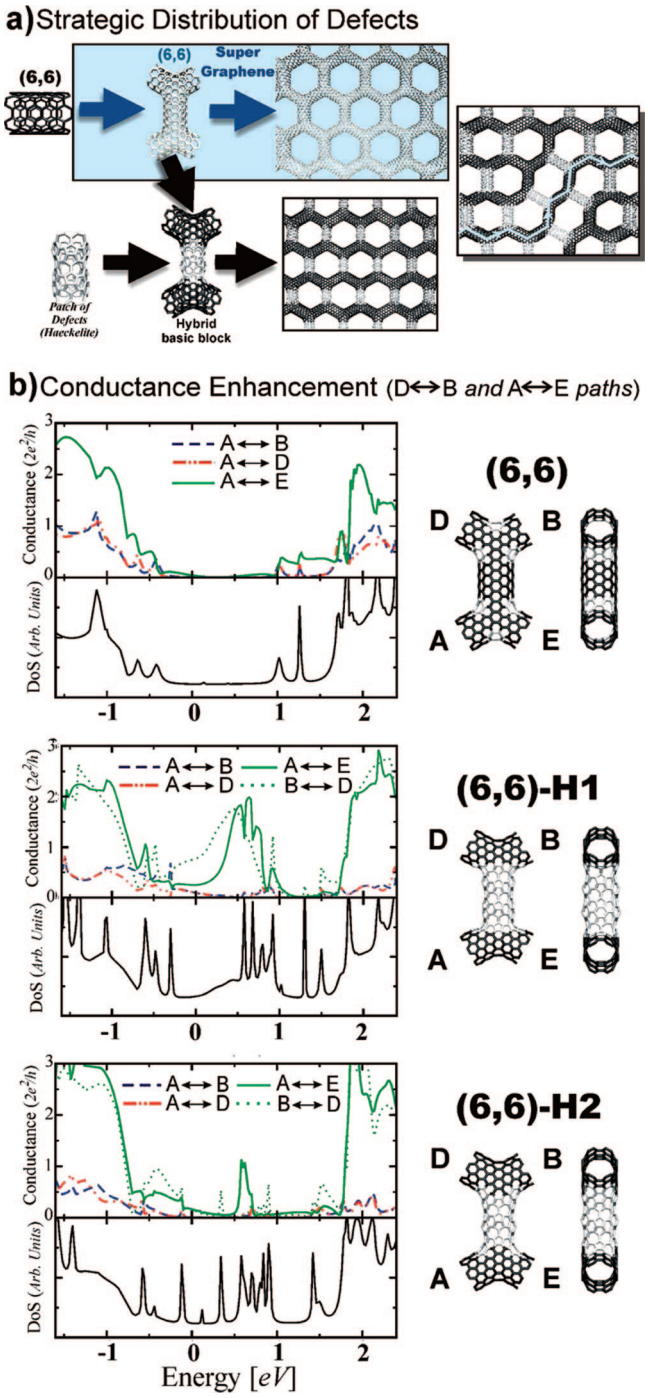

Figure 1. (a) Schematic representation of the hierarchy algorithm[19] used to strategically localize patches of defects (Haeckelites) along a network. The resulting structure is a hybrid multiterminal block. (b) (6,6) SG block and the two hybrid blocks with their conductance and DOS graphs below. An enhanced conductance around the Fermi energy is found for path A↔E and B↔D in the hybrid cases (green continuous and pointed line, respectively), due to the incorporation of patches of defects. black lines, DOS; blue dashed lines, A↔B electronic path conductance; red dashed and pointed line, A↔D electronic path conductance; green continuous line, A↔E electronic path conductance; green pointed line, B↔D electronic path conductance.

be generated by irradiation, using either an electron beam[32] or argon ion doses.[33] Another type of defect that modifies the electronic properties of nanotubes can be obtained from heterochemical doping with species such as boron,[34] nitrogen,[35] sulfur,[36] or phosphorus.[37]

In the present paper, we explore the effect of topological defects (*i.e.*, nonhexagonal rings) on the electronic transport properties of ordered networks based on carbon nanotubes (ON-CNTs). When the defects are incorporated strategically as patches within the network, they are found to adopt a behavior similar to that of intradevices, possessing the property of guiding electronic currents along specific paths through the nanomesh. This effect is studied in detail, and a general explanation of the physical phenomena governing the intradevice functions is presented.

DISCUSSION

Following the recently described hierarchy algorithm,[19] we have incorporated patches of topological defects along a number of ON-CNTs. In particular, hybrid blocks have been designed using a perfect (6,6) supergraphene (SG) block[19,20] by adding a portion of Haeckelites,[38] as schematically shown in Figure 1a. A Haeckelite structure is known as a sp^2 carbon network containing combinations of pentagonal, hexagonal, and heptagonal rings.[38] The SG architecture used in this study was specifically chosen for two reasons. First, the basic constructor block (a 4-terminal device) self-contains two nodes connected by a CNT (superbond), which allows the incorporation of patches of defects in the basic construction block. Second, the (6,6) SG block possesses conducting leads (*i.e.*, the natural way to connect the (6,6)-SG node is with (6,6)-based electrodes) due to the chirality, which indicates the presence of incoming electrons at the Fermi level. Here, two different hybrid networks, which differ by the type of Haeckelites used, were constructed. Each system exhibits a unique arrangement of the pentagons and heptagons inside the patch of defects. By comparing the results obtained with the two systems, we then studied the effect of a patch of defects on the conductance properties of the hybrid network, independently of the type of Haeckelite used (atomic models can be seen in the right column of Figure 1b, where defective rings are represented in light color).

As reported before,[44] the conductance curves exhibit a zero transmittance probability at the Fermi level for the (6,6) SG block in the absence of a patch of defects (see first graph in Figure 1b). A striking result appears once the patch of defects is incorporated: in that case we observe a large enhancement in conductance for specific paths at energies around the Fermi level (see green continuous curves in second and third conductance graphs in Figure 1b). As can be seen from the conductance graphs (Figure 1b), three inequivalent paths (A↔D, A↔B, and A↔E) are observed in the (6,6) SG block. Once the patch of defects is incorporated, the A↔E path is no longer equivalent to the D↔B one (due to a lowering of symmetry from the Haeckelites

under the mirror plane perpendicular to their axis), thus causing the appearance of four inequivalent paths (A↔D, A↔B, A↔E, and D↔B). Conductance peaks (quasi-resonances) around the Fermi energy appear for paths A↔E and D↔B, while the other two inequivalent paths A↔D and A↔B remain with zero conductance around the Fermi energy. It is remarkable that the role of the defects here is to enhance the conductance properties along specific electronic paths. This phenomenon, which is related to conservation of current in multipath systems, can be further exploited for driving electrical current through arbitrary trajectories along an ON-CNT (Figure 1a, right).

To understand the electronic process governing the observed phenomenon, a set of basic blocks was designed starting from the perfect or defect-free (6,6) SG block, and progressively incorporating generalized Stone−Wales type defects one-by-one (a total of 12 generalized Stone−Wales type defects were necessary to obtain an Haeckelite (6,6)-H1 structure). Each system was characterized with the calculations of the DOS, conductance, LDOS, and traveling electron wave function. All the structures analyzed were first relaxed using the classical Tersoff−Brenner potential, which is known to compare well with more sophisticated methods.[45] Figure 2 summarizes the conductance study, using a combination of two complementary analyses. The first analysis is performed at a "ring-level", where one ring includes four SW defects depicted in white in Figure 2a. The second analysis is carried out at a finer level of detail. In this case we investigate the systems from the 1-ring case to the 2-ring case by incorporating each individual SW defect (one-by-one) as illustrated in Figure 2b.

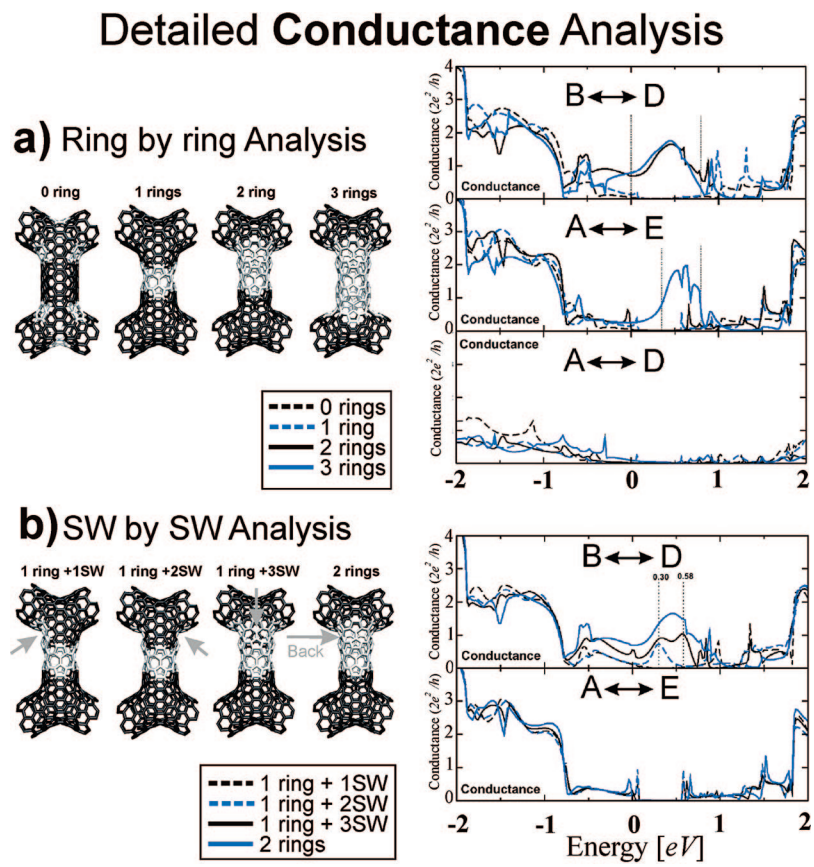

Figure 2. Top panel (a) shows the incorporation of SWs by rings (four SWs at each ring). The plot on the right shows that the increase in conductance at path B↔D appears when two and three rings are present while path A↔E presents the conductance increase when three SW rings are present. The lower panel (b) shows the incorporation of SWs one by one (defective rings marked by white color), from the first ring to the second ring. Its conductance graphs depict the conductance peaks appearing between 0.30 and 0.58 eV.

The conductance graph shown in Figure 2a corresponds the A↔E and B↔D nonequivalent electronic paths. A conductance enhancement appears for both paths between 0 and 1 eV. The increase in conductance for path B↔D appears in the 2-ring block case (solid black line in the graph) while path A↔E reveals the conductance peak in the 3-ring case (solid gray line); these quasi-resonances occur when the Stone−Wales ring is spatially closer to each electronic path, respectively. The path A↔D (*i.e.*, crossing the superbond) maintains a conductance gap. The more detailed analysis in Figure 2b presents the first conductance peak for the B↔D path at 0.30 eV, when two SWs are incorporated. A second conductance peak appears with three SWs, at 0.58 eV, and finally when the four SW defects are inserted (the second ring), both peaks merge into a broad conductance peak. The path A↔E also keeps a conductance gap as expected, since the defects were incorporated far away from the terminals.

The DOS analysis is presented in Figure 3. Here, we focus on the energy range corresponding to the energy region where the conductance is enhanced. We will concentrate on two special energy values, at 0.30 and 0.58 eV. In the analysis outlined above, we found that the concept of "patch of defects" can be used to explain the critical role played by the collective or concerted effects of multiple defects. In particular, we emphasized the critical role of charge delocalization as the driving force for current enhancement/suppression. A quasi-bound state corresponds to a localized electronic charge in space, associated with a narrow peak in the DOS curve. Likewise, the narrowness of the peak is related to a large lifetime of the electron in the state, in other words the state will typically yield a very small transmission. The physical underlying origin of those basic principles derives directly from the uncertainty or Heisenberg principle. All-in-all, the quasi-bound states are known to deteriorate the transport properties at

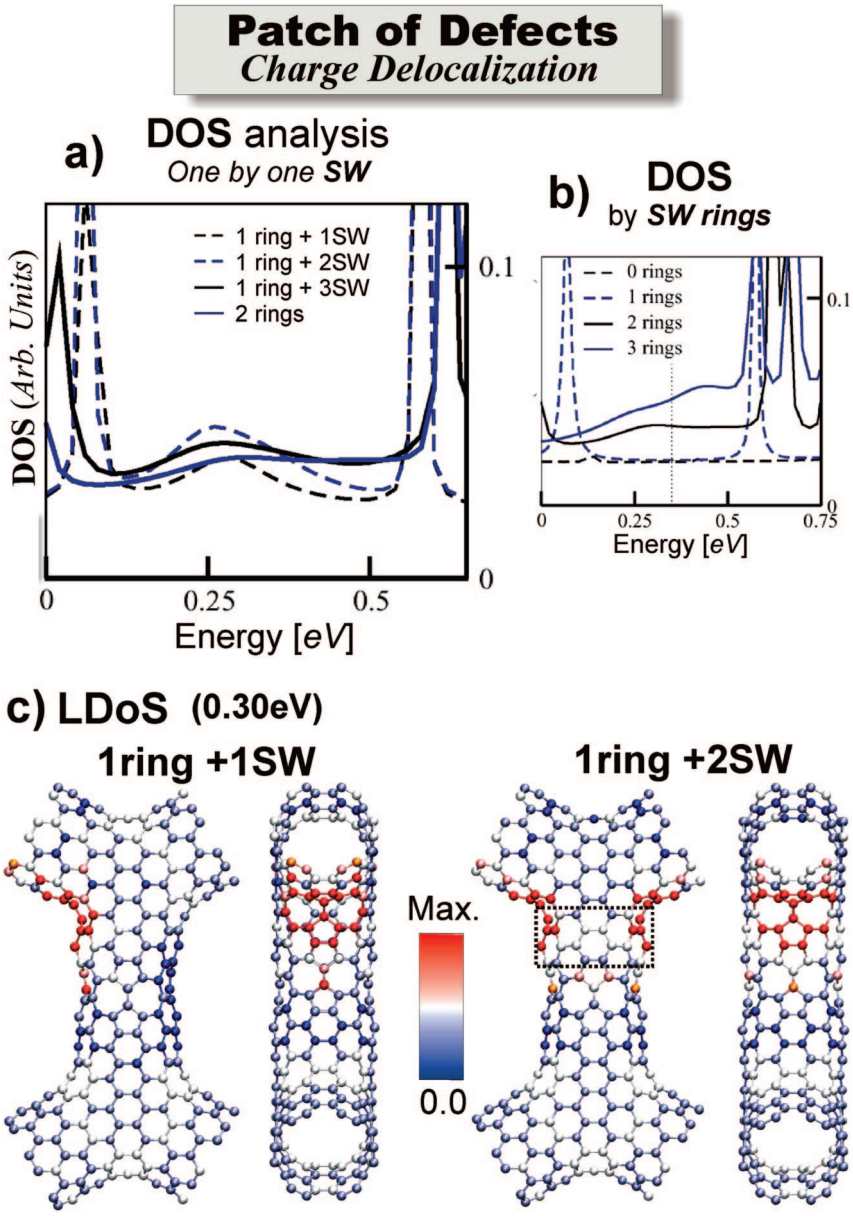

Figure 3. DOS and LDOS showing that the incorporation of a patch of defects (defects close enough to interfere) produce charge delocalization revealed here as broader peaks (quasi-bound states getting delocalized) on the energy axis at the DOS graphs. This is confirmed by the LDOS plot where the 1-ring + 2SW case shows a charge ring when the two SW defects are close enough to interfere with each other (white spots inside the dotted rectangle).

their energy[46] since the localized charge plays the role of scatterers (nontransmitting states with large lifetime). A spread peak in the energy space corresponds to a reduced lifetime and to a reduction in available quasi-momentum values (*k*-points) at the specific energy. Turning to the DOS analysis, when we follow the evolution of the peak at 0.30 eV for increasing number of defects (see left graph in Figure 3), we observe the absence of a peak when only 1-ring of SW defects is present (dashed gray line in right graph Figure 3), then a peak appears (black dashed line in left graph in Figure 3) when one SW is incorporated. As shown by the LDOS plot, the increase in electronic states is concentrated in the position of the added SW defect (red color indicating a maximum amount of electronic states). An important unusual behavior appears when two SWs are incorporated. In this case, while we observe a sharp increase in density of states, as expected, the peak starts spreading corresponding to an increase of charge delocalization. This effect is further emphasized on the LDOS plot in the 1-ring + 2SW case, where white points (inside dashed rectangle in Figure 3) are present in between both SWs defects, showing that when two SW defects are close enough their mutual influence induces charge delocalization between them. As more SW bond rotations are incorporated, the DOS peak centered at 0.30 eV keeps on spreading. A similar phenomenon is observed at 0.58 eV, where the second conductance peak appears. There is a sharp DOS peak when one and two Stone−Wales defects are incorporated (dashed curves in left graph in Figure 3). When three SWs are incorporated (which is when the conductance peak appeared), this sharp peak disappears and the increase in electronic states is distributed homogenously in the DOS curve (solid lines in left graph in Figure 3).

These observations indicate that even though an isolated SW defect generates quasi-bound states, an array of such defects close to each other (patch of defects) can induce delocalization of such electronic states, accompanied by the appearance of conductance peaks for specific electronic paths. It is worth noting that when all the possible Stone−Wales rotations are performed to obtain a Haeckelite structure, the "defects" can no longer be considered as individual defects, since they now constitute the elementary motif of the structure. It follows that the SW-induced states are now delocalized across the whole Haeckelite segment and the concept of quasi-bound states can in fact no longer be invoked, strictly speaking. Further insight can be obtained by analyzing the traveling electron wave function, at the eigen-channel level, for the two energy points of interest (0.30 and 0.58 eV).[43,44,46] Figure 4 depicts the 0.30 eV case with the LDOS of the basic block and the amplitude of the incoming traveling electron wave function (from lead B). The actual conductance values for each case presented on Figure 4 are tabulated in Table 1.

The conductance values indicate that the peak appearing when two SW defects are incorporated, originates from conduction by channel π. The wave function amplitude plots show how the traveling electron is

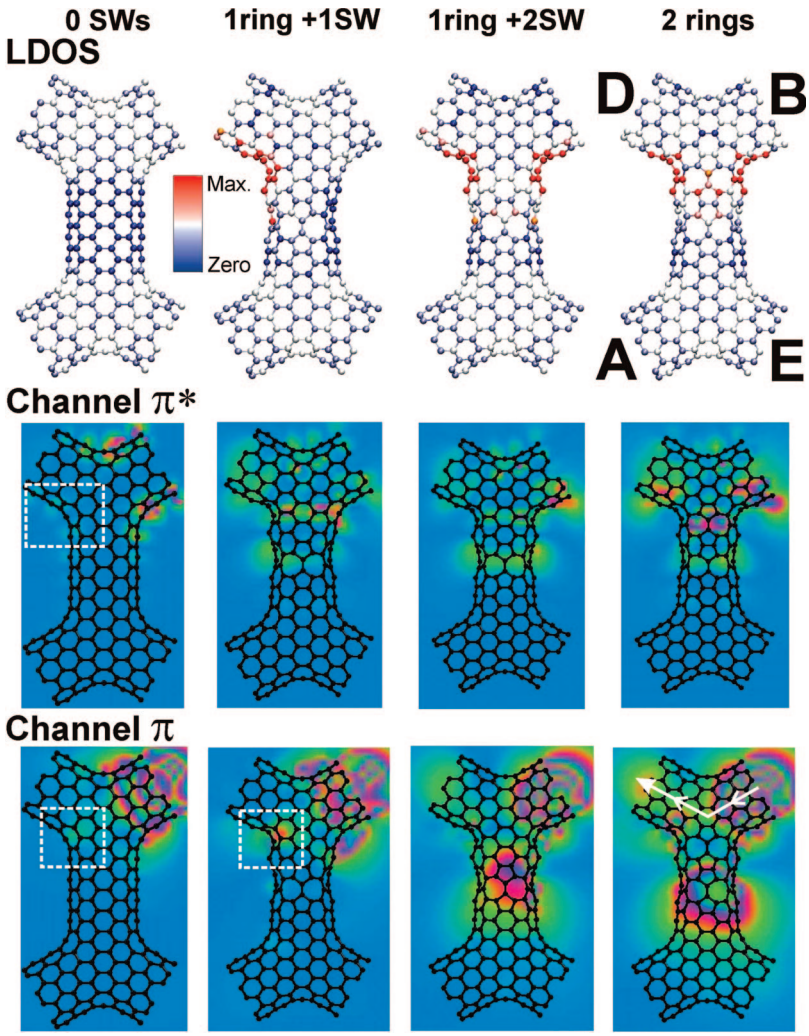

Figure 4. LDOS and scattered electron wave function analysis at $E = 0.30$ eV, where the first conductance peak appears at the 1-ring + 2SW case. The conductance (see Table 1) values indicate that the increase in conductance is due to the eigen-channel π, when two SWs interfere with each other. This collective effect caused charge delocalization into a ring which plays the role of a *bouncing barrier* for the incoming traveling electron, thereby redirecting it into the B↔D path. In the case of no added Stone−Wales defect, the incoming traveling electron is reflected by the 60° angle opposite to the incoming terminal (dashed rectangle); while with four SWs (two rings) the bouncing barrier has a stronger effect; a large portion of the wave function amplitude is redirected toward the B−D path.

reflected by the patch of defects. This reflecting effect will be denoted "bouncing" effect. When compared to the 0SW case and the 1-ring + 1SW case, we observe that in the absence of the patch of defects, the traveling electron incoming from lead B is reflected by the 60° angle composed of the two nanotubes junction at the opposite of the incoming terminal (see the dashed rectangles in channel π plots) without any bouncing effect. When the second ring of SW defects is fully incorporated, the bouncing effect of the traveling electron is improved increasing the conductance through path D↔B. These observations suggest that the patch of defects promotes the reflection (bouncing effect) of the traveling electron, leading the incoming electron to leave the multiterminal device by terminal D (*i.e.*, different from the incoming terminal), thereby increasing the conductance through this specific path. When the second ring is fully incorporated, the charge in the middle ring decreases and becomes delocalized into the full patch including the upper ring (see channel π* plots; complemented by LDOS plot), which leads to an improvement of the conductance through this channel by reflecting (bouncing) part of the charge coming with the traveling electron from lead B to lead D on channel π*. This analysis based on the scattering wave function decomposition of the conductance confirms the analysis based on LDOS and further highlights the key concerted role of multiple defects.

TABLE 1. Conductance Values from the Eigen-Channel Analysis at $E = 0.30$ eV[a]

	B↔D		A↔E	
	channel π* $k = 1.92/ao$	channel π $k = 2.20/ao$	channel π*	channel π
1-ring + 1SW	0.00	0.00	0.00	0.01
1-ring + 2SW	0.00	0.72	0.00	0.01
1-ring + 3SW	0.14	0.75	0.00	0.01
2-rings	0.45	0.89	0.00	0.01

[a] A conductance increase for path B↔D from eigen-channel π was observed since 1-ring + 2SW are present. The electronic path A↔E maintains zero conductance as expected since the SW defects rings are far away from such terminals.

CONCLUSION

In summary, we have shown that structural alterations, when strategically incorporated as patches of defects along carbon nanotube networks, can be used to program a complex nanotube circuit to enhance the conductance along specific paths. We demonstrated that while single defects are characterized by the presence of quasi-bound states, patches of defects lead to a charge delocalization, which is accompanied by a "bouncing" phenomena that redirects the incoming traveling electrons to a

given trajectory. The theoretical predictions presented here should motivate dedicated experimental work to explore the feasibility of assembling covalent ordered networks based on CNTs as a crucial step for the future of nanoelectronics. For example, using electron or ion irradiation on specific sites of nanotube networks could be used to create patches of defects in desired sites, thus controlling the electron transport and the operation of the nanotube device.

METHOD

The electronic transport properties were calculated with the Landauer−Buttiker formalism[39−41] and equilibrium Green functions, taking curvature into account by a semiempirical Hamiltonian based on four orbitals (s, p_x, p_y, p_z) per carbon atom.[42] The study of the scattered wave functions was carried out using a methodology used previously in ref 43. Details of the methods used are reported in ref 44.

Acknowledgment. A portion of this research was conducted at the Center for Nanophase Materials Sciences, which is sponsored at Oak Ridge National Laboratory by the Division of Scientific User Facilities, U.S. Department of Energy. V.M. also acknowledges the Division of Materials Science, U.S. Department of Energy under Contract No. DEAC05-00OR22725 with UT-Battelle, LLC at Oak Ridge National Laboratory. This work was supported by CONACYT-México grants 56787 (Laboratory for Nanoscience and Nanotechnology Research-LINAN), 45762 (H.T.), 45772 (M.T.), 41464-Inter American Collaboration (M.T.), 42428-Inter American Collaboration (H.T.), 2004-01-013/SALUD-CONACYT (M.T.), Fondo Mixto de San Luis Potosí 63001 S-3908 (M.T.), Fondo Mixto de San Luis Potosí 63072 S-3909 (H.T.), and Ph.D. Scholarhsip (J.M.R.H.). We also acknowledge Special Scholarship by IPICyT scholarships grant (J.M.R.H.). We are very thankful to Daniel Ramírez and Grisel Ramírez for technical support.

REFERENCES AND NOTES

1. Winfree, E.; Liu, F.; Wenzler, L. A.; Seeman, N. C. Design and Self-assembly of Two-Dimensional DNA crystals. *Nature* **1998**, *394*, 539–544.
2. Chworos, A.; Severcan, I.; Koyfman, A. Y.; Weinkam, P.; Oroudjev, E.; Hansma, H. G.; Jaeger, L. Building Programmable Jigsaw Puzzles with RNA. *Science* **2004**, *306*, 2068–2072.
3. Seeman, N. C. DNA in a Material World. *Nature* **2003**, *421*, 427–431.
4. Kalsin, A. M.; Fialkowski, M.; Paszewski, M.; Smoukov, S. K.; Bishop, K. J. M.; Grzybowski, B. A. Electrostatic Self-Assembly of Binary Nanoparticle Crystals with a Diamond-Like Lattice. *Science* **2006**, *312*, 420–424.
5. Shevchenko, E. V.; Talapin, D. V.; Kotov, N. A.; O'Brien, S.; Murray, C. B. Structural Diversity in Binary Nanoparticle Superlattices. *Nature* **2006**, *439*, 55–59.
6. Redl, F. X.; Cho, K.-S.; Murray, C. B.; O'Brien, S. Three-Dimensional Binary Superlattices of Magnetic Nanocrystals and Semiconductor Quantum Dots. *Nature* **2003**, *423*, 968–971.
7. Huang, Y.; Duan, X.; Wei, Q.; Lieber, C. M. Directed Assembly of One-Dimensional Nanostructures into Functional Networks. *Science* **2001**, *291*, 630–633.
8. Whang, D.; Jin, S.; Wu, Y.; Lieber, C. M. Large-Scale Hierarchical Organization of Nanowire Arrays for Integrated Nanosystems. *Nano Lett.* **2003**, *3*, 1255–1259.
9. Tao, A.; Kim, F.; Hess, C.; Goldberger, J.; He, R. R.; Sun, Y. G.; Xia, Y. N.; Yang, P. D. Langmuir−Blodgett Silver Nanowire Monolayers for Molecular Sensing Using Surface-Enhanced Raman Spectroscopy. *Nano Lett.* **2003**, *3*, 1229–1233.
10. Tans, S. J.; Devoret, M. H.; Dai, H. J.; Thess, A.; Smalley, R. E.; Geerligs, L. J.; Dekker, C. Individual Single-Wall Carbon Nanotubes as Quantum Wires. *Nature* **1997**, *386*, 474–477.
11. Chico, L.; Crespi, V. H.; Benedict, L. X.; Louie, S. G.; Cohen, M. L. Pure Carbon Nanoscale Devices: Nanotube Heterojunctions. *Phys. Rev. Lett.* **1996**, *76*, 971–974.
12. Yao, Z.; Postma, H.W.Ch.; Balents, L.; Dekker, C. Carbon Nanotube Intramolecular Junctions. *Nature* **1999**, *402*, 273–276.
13. Tans, S. J.; Verschueren, A. R. M.; Dekker, C. Room-Temperature Transistor Based on a Single Carbon Nanotube. *Nature* **1998**, *393*, 49–52.
14. Derycke, V.; Martel, R.; Appenzeller, J.; Avouris, P. Carbon Nanotube Inter- and Intramolecular Logic Gates. *Nano Lett.* **2001**, *1*, 453–456.
15. Hayden, O.; Agarwal, R.; Lieber, C. M. Nanoscale Avalanche Photodiodes for Highly Sensitive and Spatially Resolved Photon Detection. *Nat. Mater.* **2006**, *5*, 352–356.
16. Duan, X.; Huang, Y.; Lieber, C. M. Nonvolatile Memory and Programmable Logic from Molecule-Gated Nanowires. *Nano Lett.* **2002**, *2*, 487–490.
17. Huang, Y.; Duan, X. F.; Cui, Y.; Lauhon, L. J.; Kim, K. H.; Lieber, C. M. Logic Gates and Computation from Assembled Nanowire Building Blocks. *Science* **2001**, *294*, 1313–1317.
18. Zhong, Z.; Wang, D.; Cui, Y.; Bockrath, M. W.; Lieber, C. M. Nanowire Crossbar Arrays as Address Decoders for Integrated Nanosystems. *Science* **2003**, *302*, 1377–1379.
19. Romo-Herrera, J. M.; Terrones, M.; Terrones, H.; Sag, S.; Meunier, V. Covalent 2D and 3D Networks from 1D Nanostructures: Designing New Materials. *Nano Lett.* **2007**, *7*, 570–576.
20. Colucci, V. R.; Galvao, D. S.; Jorio, A. Geometric and Electronic Structure of Carbon Nanotube Networks: 'Super'-Carbon Nanotubes. *Nanotechnology* **2006**, *17*, 617–621.
21. Rueckes, T.; Kim, K.; Joselevich, E.; Tseng, G. Y.; Cheung, C. L.; Lieber, C. M. Carbon Nanotube-Based Nonvolatile Random Access Memory for Molecular Computing. *Science* **2000**, *289*, 94–97.
22. Ismach, A.; Joselevich, E. Orthogonal Self-Assembly of Carbon Nanotube Crossbar Architectures by Simultaneous Grapho Epitaxy and Field-Directed Growth. *Nano Lett.* **2006**, *6*, 1706–1710.
23. Terrones, M.; Banhart, F.; Grobert, N.; Charlier, J. C.; Terrones, H.; Ajayan, P. M. Molecular Junctions by Joining Single-Walled Carbon Nanotubes. *Phys. Rev. Lett.* **2002**, *89*, 075505-1–075505-4.
24. Endo, M.; Muramatsu, H.; Hayashi, T.; Kim, Y. A.; Van Lier, G.; Charlier, J. C.; Terrones, H.; Terrones, M.; Dresselhaus, M. S. Atomic Nanotube Welders: Boron Interstitials Triggering Connections in Double-Walled Carbon Nanotubes. *Nano Lett.* **2005**, *5*, 1099–1105.
25. Chuanhong, J.; Suenaga, K.; Iijima, S. Plumbing Carbon Nanotubes. *Nat. Nanotechnol.* **2008**, *3*, 17–21.
26. Crespi, V. H.; Cohen, M. L.; Rubio, A. In Situ Band Gap Engineering of Carbon Nanotubes. *Phys. Rev. Lett.* **1997**, *79*, 2093–2096.
27. Chico, L.; Benedict, L. X.; Louie, S. G.; Cohen, M. L. Quantum Conductance of Carbon Nanotubes with Defects. *Phys. Rev. B* **1996**, *54*, 2600–2606.
28. Stone, A. J.; Wales, D. J. Theoretical Studies of Icosahedral C_{60} and some Related Species. *Chem. Phys. Lett.* **1986**, *128*, 501–503.
29. Orlikowski, D.; Nardelli, M. B.; Bernholc, J.; Roland, C. Add-dimers on Strained Carbon Nanotubes: A New Route for Quantum Dot Formation. *Phys. Rev. Lett.* **1999**, *83*, 4132–4135.

30. Chico, L.; López Sancho, M. P.; Muñoz, M. C. Carbon-Nanotube-Based Quantum Dot. *Phys. Rev. Lett.* **1998**, *81*, 1278–1281.
31. Meunier, V.; Nardelli, M. B.; Roland, C.; Bernholc, J. Structural and Electronic Properties of Carbon Nanotube Tapers. *Phys. Rev. B* **2001**, *64*, 195419-1–195419-7.
32. Ajayan, P. M.; Ravikumar, V.; Charlier, J.-C. Surface Reconstructions and Dimensional Changes in Single-Walled Carbon Nanotubes. *Phys. Rev. Lett.* **1998**, *81*, 1437–1440.
33. Gomez-Navarro, C.; De Pablo, P. J.; Gomez-Herrero, J.; Biel, B.; Garcia-Vidal, F. J.; Rubio, A.; Flores, F. Tuning the Conductance of Single-walled Carbon Nanotubes by Ion Irradiation in the Anderson Localization Regime. *Nat. Mater.* **2005**, *4*, 534–539.
34. Carroll, D. L.; Redlich, P.; Blase, X.; Charlier, J. C.; Curran, S.; Ajayan, P. M.; Roth, S.; Ruhle, M. Effects of Nanodomain Formation on the Electronic Structure of Doped Carbon Nanotubes. *Phys. Rev. Lett.* **1998**, *81*, 2332–2335.
35. Czerw, R.; Terrones, M.; Charlier, J. C.; Blase, X.; Foley, B.; Kamalakaran, R.; Grobert, N.; Terrones, H.; Tekleab, D.; Ajayan;, P.; *et al*. Identification of Electron Donor States in N-Doped Carbon Nanotubes. *Nano Lett.* **2001**, *1*, 457–460.
36. Romo-Herrera, J. M.; Sumpter, B. G.; Cullen, D. A.; Terrones, H.; Cruz-Silva, E.; Smith, D. J.; Meunier, V.; Terrones, M. An Atomistic Branching Mechanism for Carbon Nanotubes: Sulfur as the Triggering Agent. *Angew. Chem., Int. Ed.* **2008**, *47*, 2948–2953.
37. Cruz-Silva, E.; Cullen, D. A.; Gu, L.; Romo-Herrera, J. M.; Munoz-Sandoval, E.; Lopez-Urias, F.; Sumpter, B. G.; Meunier, V.; Charlier, J. C.; Smith, D. J.; *et al.* Heterodoped Nanotubes: Theory, Synthesis, and Characterization of Phosphorus Nitrogen Doped Multiwalled Carbon Nanotubes. *ACS Nano* **2008**, *2*, 441–448.
38. Terrones, H.; Terrones, M.; Hernández, E.; Grobert, N.; Charlier, J.-C.; Ajayan, P. M. New Metallic Allotropes of Planar and Tubular Carbon. *Phys. Rev. Lett.* **2000**, *84*, 1717–1719.
39. Landauer, R. Electrical Resistance of Disordered One-Dimensional Lattices. *Philos. Mag.* **1970**, *21*, 863.
40. Büttiker, M. Four-Terminal Phase-Coherent Conductance. *Phys. Rev. Lett.* **1986**, *57*, 1761–1764.
41. Datta, S. *Electronic Transport in Mesoscopic Systems*; Cambridge University Press: Cambridge, U.K. 1995.
42. Charlier, J.-C.; Lambin, Ph.; Ebbesen, T. W. Electronic Properties of Carbon Nanotubes with Poligonized Cross Sections. *Phys. Rev. B* **1996**, *54*, R8377–R8380.
43. Meunier, V.; Kalinin, S. V.; Sumpter, B. G. Nonvolatile Memory Elements Based on the Intercalation of Organic Molecules Inside Carbon Nanotubes. *Phys. Rev. Lett.* **2007**, *98*, 056401-1–056401-4.
44. Romo-Herrera, J. M.; Terrones, M.; Terrones, H.; Meunier, V. Electron Transport Properties of Ordered Networks using Carbon Nanotubes. *Nanotechnology* **2008**, *19*, 315704.
45. Brenner, D. W. Empirical Potential for Hydrocarbons for use in Simulating the Chemical Vapor Deposition of Diamond Films. *Phys. Rev. B* **1990**, *42*, 9458–9471.
46. Rubio, A.; Sanchez-Portal, D.; Artacho, E.; Ordejon, P.; Soler, J. M. Electronic Status in a Finite Carbon Nanotube: A One-Dimensional Quantum Box. *Phys. Rev. Lett.* **1999**, *82*, 3520–3523.